The First Layers of Water on Ru(001)

Y. Lilach, L. Romm, T. Livneh, and M. Asscher*

Department of Physical Chemistry and the Farkas Center for Light Induced Processes, The Hebrew University, Jerusalem 91904, Israel

Received: September 27, 2000; In Final Form: January 16, 2001

The initial growth of water molecules to form the first bilayer and then ice layers on Ru(001) was studied utilizing work function change ($\Delta\Phi$), temperature programmed desorption (TPD), and supersonic atomic beam−collision-induced desorption (CID) measurements. A kinetic model that reproduces the first bilayer growth, as determined by the $\Delta\Phi$ measurements, was developed. It indicates that monomers dominate the cluster size distribution at low coverages, but at high coverages, tetramers gradually become the dominant clusters. Small contributions to $\Delta\Phi$ suggest that tetramers are cyclic at the adsorbed state with inclined dipoles. CID measurements of H_2O and D_2O at coverages near one bilayer reveal strong selectivity to the removal of molecules in the A_2 adsorption sites over those in the icelike C sites and the A_1 sites. Soft removal rates of thicker ice layers as a result of CID with energetic Kripton atoms were then studied as a function of the ice layer thickness. Near the completion of the third bilayer, a sharp stabilization of the ice structure occurs, which leads to two concomitant effects: (a) a significant decrease in the CID removal rate of the ice layers, and (b) caging of adsorbed nitrogen followed by an extremely sharp desorption of the trapped molecules near 165 K. This happens at the onset of the ice desorption temperature. These effects are discussed in terms of the structure of the first layers of ice which grow on the surface of a Ru(001) single crystal and are consistent with recent model molecular dynamics simulations of such a system.

1. Introduction

The structure of water molecules on metal surfaces has been the subject of extensive research in recent years.[1−23] This is partly due to the unique hydrogen bonding among neighbor adsorbates on the surface, which is similar to the binding energy of the molecule to the metal. In addition, the possible catalytic role of stratospheric ice particles on the destruction of the ozone layer has stimulated further research on ice particles supported on well-defined surfaces. The specific case of water on Ru(001) received special attention[7−23] since there is close similarity between the unit cell dimensions of the (001) plane of Ru and that of hexagonal ice. The structure of the first bilayer of water on Ru(001) was very carefully studied by a video−LEED technique[9,20] and found to have a different structure than that suggested before.[10] The LEED analysis suggests that oxygen atoms in the second layer are only 0.1 Å further removed from the metal plane than the oxygen atoms that pertain to molecules of the first layer. In addition, significant buckling of the respective metal atoms has been proposed. The previous understanding was that the oxygen atoms of the second layer molecules within the first bilayer adsorb 0.96 Å higher than those of the first layer atoms to preserve the hydrogen-bonding rules defined by Bernal, Fowler, and Pauling.[24,25] In addition, an interesting and unique kinetic isotope effect in desorption has been reported,[13,19] where the high-temperature desorption peak − A_1 practically does not exist in the desorption of D_2O. In contrast, when adsorbing H_2O, the A_1 state is clearly resolved and was thought to arise from A_2 molecules upon sample heating.[13] The LEED study claimed that the origin of the kinetic isotope effect is in microscopic structural differences between D_2O and H_2O when adsorbed on Ru(001).[19]

The possible effect of collisions of energetic gas atoms and molecules on the interaction and chemistry of adsorbates has been studied in recent years, for, among other reasons, their relevance to industrial high-pressure heterogeneous catalysis.

The dynamical aspects of such energetic collisions were discussed theoretically for the first time by Zeiri et al.[26] who employed classical trajectory simulations to study the desorption of Xe and nitrogen adsorbates as a function of collider energy and angle of incidence. Experiments were performed for the first time by Ceyer and co-workers,[27] who reported the collision-induced desorption (CID) and dissociation of CH_4 on Ni(111). Since then, other adsorbate−surface systems were studied as well, including the CID of NH_3 and C_2H_4 from Pt(111),[28] O_2 from Ag(100)[29] and Pt(111).[30] We have recently completed a CID study of N_2 from Ru(001), combining the experimental work with MD simulations in order to have better insight into the microscopic CID dynamics.[31,32] A preliminary study of the CID of water from Ru(001) was published earlier.[23]

Here, we present an attempt to analyze the results of a CID study, combined with work function and TPD in order to understand structural details which pertain to the initial growth of water molecules and ice on Ru(001).

2. Experimental Section

The collision-induced desorption measurements reported here were performed in a UHV chamber attached to a supersonic beam source having two stages of differential pumping.[23] A ceramic nozzle with an orifice of 70 μm could be heated to 1800 K. The chamber is equipped with standard surface cleaning and characterization tools and is operated at a base pressure below $2 \cdot 10^{-10}$ Torr, rising to $1 \cdot 10^{-8}$ Torr when the beam is on. The rare gas atoms (Kr and Ar) were seeded in He carrier gas, and the beam formed was chopped at 400 Hz using a vacuum compatible, miniature synchronous motor (Condor

10.1021/jp003511g CCC: $20.00
Published on Web 03/17/2001

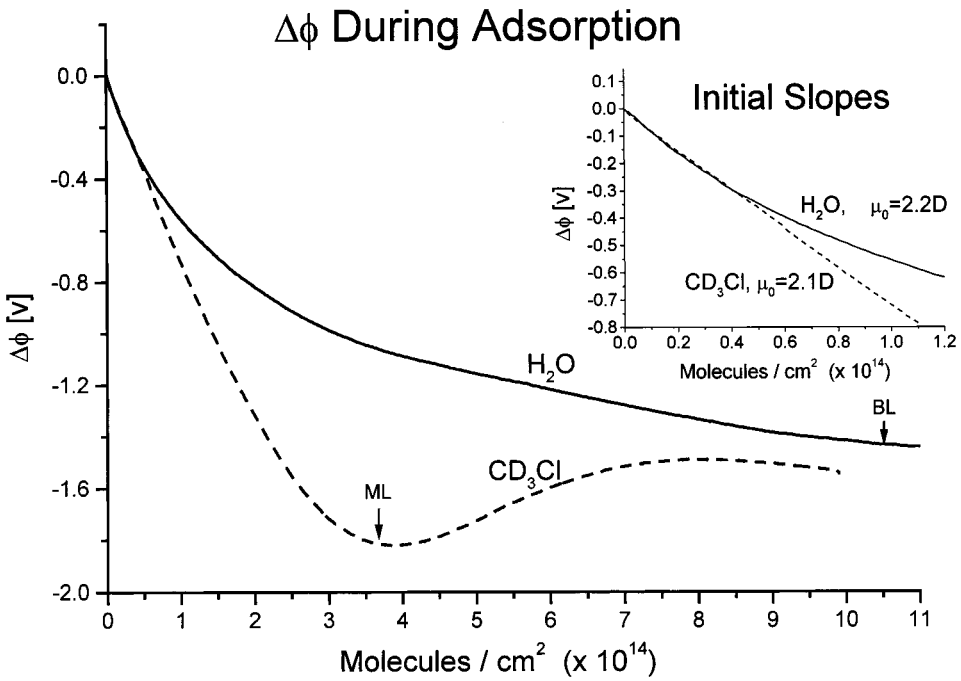

Figure 1. Work function change ($\Delta\varphi$) of water and methyl chloride vs accumulated surface density (total number of adsorbates per cm^2) on Ru(001) at surface temperature of 82 K. The densities equivalent to 1 ML CD_3Cl and 1 BL H_2O are marked as arrows. In the inset, $\Delta\varphi$ at low coverages is shown. The dipole moment for both adsorbed molecules is extracted from the initial slopes.

Pacific, Inc.) for time-of-flight measurements to determine the incident energy of the colliders. The flux of 2% Kr atoms seeded in He has been determined to be $(1 \pm 0.5) \cdot 10^{14}$ atoms/cm^2 s. Kinetic energy spread $\Delta E/E$ (at half-maximum) of 0.20 was measured at kinetic energies less than 1.0 eV, increasing to 0.25 at higher energies. The beam size is slightly larger than the crystal so that the colliders strike uniformly the entire surface.

High-purity $^{15}N_2$ without further cleaning has been used to reduce background problems in the nitrogen caging experiments and for post-CID, clean surface titration measurements. Triple-distilled water and nominally 98% pure D_2O were used. However, after being in the stainless steel tubing, measurements with the quadrupole revealed that the D_2O was only 75% pure. Exposure was done directly from a leak valve, calibrated for ion gauge sensitivity. Work function measurements were performed in a separate UHV chamber on a different Ru(001) crystal. TPD of H_2O from the two crystals were practically identical, except for small differences in crystal temperature measurements. A Kelvin probe (Besocke, Kelvin probe −S) has been mounted on a translation stage, with its gold reference electrode shielded against sputter and other evaporation impurities. The output voltage has been digitized and input to a computer to enable coupling to the TPD routine. This way $\Delta\varphi$−TPD measurements could be obtained with a resolution of 5 meV.[23] All TPD runs were performed in a constant heating rate of 2 K/s. Very sharp LEED spots with the proper hexagonal symmetry were obtained from the clean Ru(001) crystal. Surface cleanliness and chemical composition were determined by Auger spectroscopy.

3. Results and Discussion

3.1. Initial Growth of Water Molecules on Ru(001) at 82 K. Work function change measurements ($\Delta\varphi$) were performed during adsorption of water molecules in order to follow the initial growth on the clean Ru(001) surface at 82 K. In Figure 1, the rapid change in work function is recorded continuously while exposing the surface to water vapor. The work function change is plotted against the surface density of the adsorbed molecules. The surface density of water molecules is estimated from the onset of ice desorption near 150−160 K, which is found at an exposure of 0.9 L (1 L = 10^{-6} Torr s) and corresponds to 1.05×10^{15} molecules/cm^2.[19,23] The initial slope of the curve of water $\Delta\varphi$ versus density is compared with that of methyl chloride. It is correlated with the dipole moment of the adsorbed molecules via the Helmholtz expression, which is expected to be accurate at very low coverages: $\Delta\varphi = -4\pi N\mu_0$, where N is the adsorbed molecules density and μ_0 is their initial (close to zero coverage) dipole moment.

Water and methyl chloride have practically the same dipole moment in the gas phase (1.88 ± 0.02 D). The adsorbed molecules also have very similar dipole moment of 2.15 ± 0.1 D near zero coverage. While the dipole moment of adsorbed methyl chloride (as indicated from the linear initial slope of the curve in the inset of Figure 1) seems constant and does not change significantly with coverage (at low coverage), the behavior of water is rather different. At coverages as low as 0.02 BL, the $\Delta\varphi$ curve is already bending over, indicating the onset of dipole moment change practically immediately. The origin of this behavior needs to be addressed. One possible explanation is the formation of water clusters on the surface upon adsorption that affect the average dipole moment. IR measurements indeed indicate that monomers and tetramers are stable on Ru(001) at temperatures below 100 K.[22]

To analyze the initial slope of the curve in Figure 1 as coverage increases, we have employed a kinetic model that considers a clustering process upon adsorption of water molecules from the gas phase. Coupled rate equations, describing the formation of each of the clusters (N_i, $i = 1-4$), were numerically integrated to obtain the density of each of these clusters at any given exposure. We limited the cluster size to tetramers in order to be consistent with the IR measurements mentioned above.[22] The resulting sum of density times the contribution to the work function change ($\Delta\varphi_i$) of each of these clusters via their dipole moment (μ_i) is plotted against the

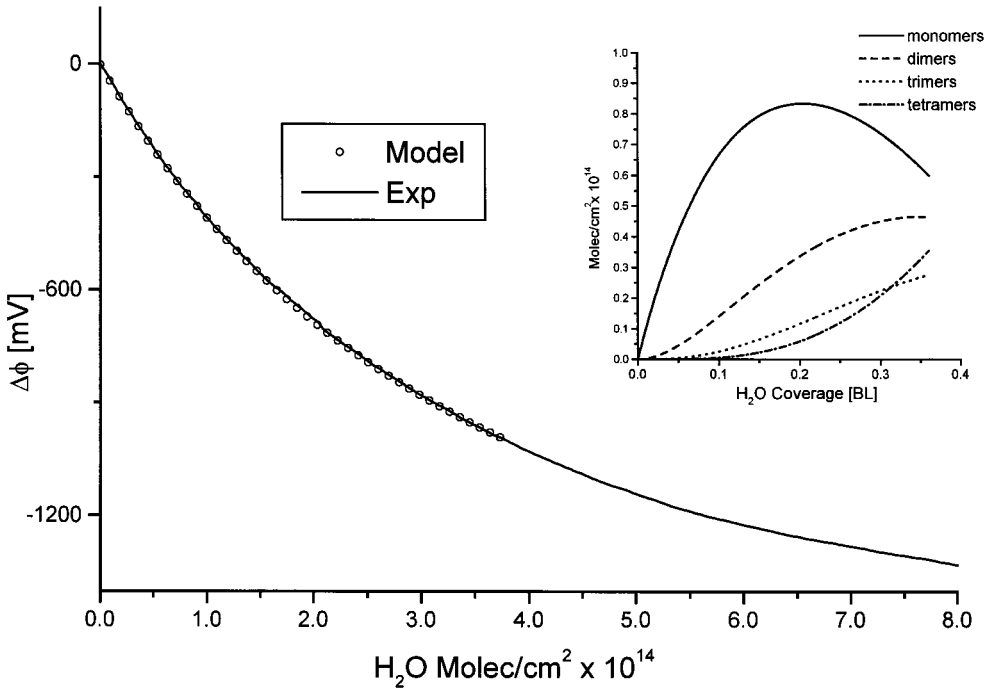

Figure 2. Work function change ($\Delta\varphi$) of water vs accumulated surface density. Open circles represent the calculated $\Delta\varphi$ using the kinetic model described in the text. In the inset, the density of the water clusters derived from the kinetic model is shown as they vary with the number of H_2O bilayers.

experimental $\Delta\varphi$ curve in Figure 2. A definition of the dipole moment of an isolated adsorbed water molecule (monomer) can be obtained from the slope of the curve in Figure 1 as coverage approaches zero. The dipole moments pertaining to the various clusters are as follows: $\mu_1 = 2.20$ D, $\mu_2 = 1.12$ D, $\mu_3 = 0.86$ D, $\mu_4 = 0.92$ D. The rate constant for the formation of the monomers (k_1) was $0.9 \cdot 10^{-15}$ cm^2/molecule, slightly smaller than the (same) rates for the formation of the larger clusters, all having the same value, $k_{2-4} = 1.38 \cdot 10^{-15}$ cm^2/molecule. Details of the kinetic model are given elsewhere.[38]

The calculated work function change is eventually obtained at any stage of the exposure by the following expression:

$$\Delta\varphi_{\text{calc}} = N_1\Delta\varphi_1 + N_2\Delta\varphi_2 + N_3\Delta\varphi_3 + N_4\Delta\varphi_4 \qquad (1)$$

where $\Delta\varphi_i$ are the contributions to the work function change of each of the clusters, due to their specific dipole moments, μ_i (via the Helmholtz equation mentioned above). The resulting work function change is plotted versus the surface density in Figure 2 (open circles) together with the experimental data (solid line). In the inset of Figure 2, the number density of each of the clusters is shown versus the surface coverage.

The actual cluster sizes existing on the Ru(001) at 82 K cannot be determined solely by work function measurements. However, the fact that in our kinetic model tetramers become the most abundant clusters above a coverage of 0.4 BL seems to agree with the IR study that reported the presence and dominance of this cluster.[22] On the other hand, our model disagrees with this report's claim that only monomers and tetramers are stable on the Ru(001) surface at 100 K. Our kinetic model suggests that mono-, di-, and trimers are all residing on the surface at the same time, although at coverages below 0.05 BL, only mono- and dimers are found.

It is interesting to note that the contribution to the work function change by tri- and tetramers is relatively small. This implies that the overall dipole moment is dictated mainly by the mono- and dimers and that tri- and tetramers do not have large dipole moments. This implies a cyclic and tilted geometry of the three or four water molecules that form the clusters on the surface such that their dipole is minimal. Such a geometry can be understood if both the bonding to the metal through the oxygen atom and the intermolecular hydrogen bonding are simultaneously kept. Cyclic geometry of water clusters $(H_2O)_n$ in the size range $n = 3-5$ in the gas phase have been conclusively demonstrated based on OH stretch frequency measurements.[33]

3.2. TPD of H_2O and D_2O from Ru(001). TPD spectra of H_2O and D_2O following adsorption of 1.1 bilayer (1 BL = 1.05×10^{15} molecules/cm^2) on Ru(001) at temperatures of 90 and 140 K are shown in Figure 3. These spectra were taken at a heating rate of 2 K/s. Only a small shoulder near 205 K (A_1 state) is observed in the desorption spectrum of D_2O, but it clearly appears in the case of H_2O. It was claimed in the literature[17,20] that there is no thermal way to significantly populate the A_1 state during the TPD of D_2O. It is interesting to note that at all adsorption temperatures below 140 K and at all exposures, a small desorption peak appears near 150−160 K. This peak is believed to arise from small 3D water (ice) clusters formed on the surface before or during the TPD run. This peak slowly increases with exposure and shifts toward 165 K as coverage increases. It eventually merges with the C state, which represents desorption from an icelike layer. Work function change measurements performed during temperature sweep in a $\Delta\varphi-$TPD mode are shown in Figure 4. The spectrum reveals a clear contribution to the work function from each of the normal TPD desorption peaks. Differentiation of the $\Delta\varphi-$TPD signals versus temperature ($d\Delta\varphi/dT$), generates desorption-like spectra. It is interesting to note that the peak that pertains to the $d\Delta\varphi/dT$ A_2 molecules is significantly shifted to higher temperatures compared with that obtained in the normal $\Delta p-$TPD spectrum. The origin of this shift is not clear. One possible explanation is that there are molecules that desorb within the A_2 state which are more weakly bound and thus not oriented perpendicular to the surface. These molecules desorb at lower temperature and

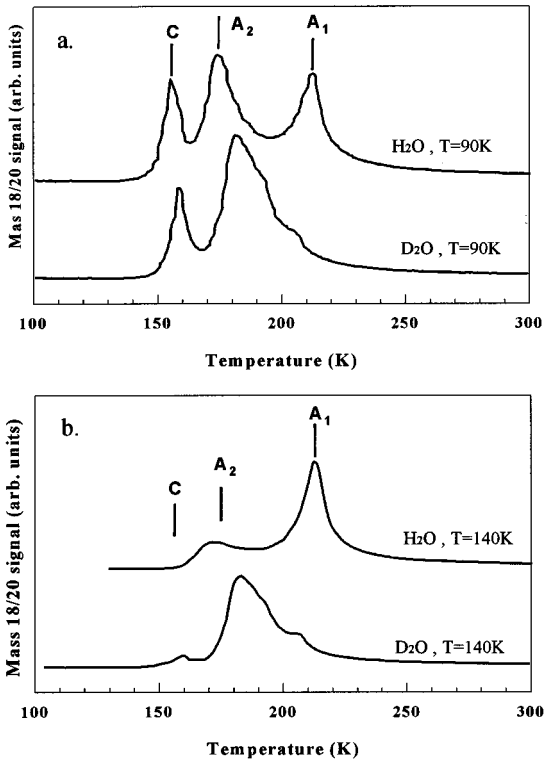

Figure 3. TPD of H_2O and D_2O from Ru(001) following adsorption of 1.1 BL on Ru(001) at 90 (a) and 140 K (b). The heating rate was 2 K/s.

are not expected to contribute significantly to the work function change. As a result, the A_2 $\Delta\varphi-$TPD peak shifts to higher temperatures compared with the corresponding $\Delta p-$TPD peak. This explanation is supported by the fact that at lower coverages, the A_2 $\Delta p-$TPD peak diminishes significantly faster than the corresponding $d\Delta\varphi/dT$ peak, as demonstrated in Figure 4 for coverages of 1.1, 0.4, and 0.2 BL. At the lowest coverage in which the weaker bound molecules do not exist, the A_2 TPD peaks obtained by the two different modes overlap. The model that explains the shift in the A_2 $d\Delta\varphi/dT$ peak to high temperature is nicely consistent with our kinetic model discussed in section 3.1 above. In that model, the contribution to the work function change of tetramers, that are dominant at higher coverages, is also predicted to be negligible.

Another interesting observation in the $d\Delta\varphi/dT$ spectrum is the contribution to the measured work function change from molecules desorbing around 150−160 K, attributed to icelike particles that form 3D clusters. It means that molecules that reside several layers above the surface still affect the measured work function. It was shown before in the adsorption of CH_3-BR and CH_3Cl on Ru(001)[34] that molecules up to the third layer can still affect the measured work function. In addition, the fact that, during adsorption of water, work-function change can be detected up to a coverage of 2.5−3 BL suggests that partial orientation of the adsorbed water molecules is preserved relatively far from the surface in this hydrogen-bonded network. It implies that the water molecules may form ferroelectric-like layers and are not fully amorphous with random orientation of the hydrogen atoms at least up to 3 BL coverage.[21] A similar shift to higher temperature as in the high coverage A_2 $d\Delta\varphi/dT$ spectrum is also seen in the C desorption peak of the icelike particles near 150−160 K.

3.3. CID of H_2O and D_2O from Ru(001). TPD spectra are shown in Figure 5 following collision-induced desorption of H_2O and D_2O from Ru(001) by Kr atoms (seeded in He) at kinetic energy of 4.6 eV. Initial water exposure was equivalent to the formation of 1 BL at crystal temperature of 140 K. Similar results were obtained after water adsorption at crystal temperature of 90 K, except for the presence of an extra icelike C peak. The results of the CID, as revealed by the post-collision

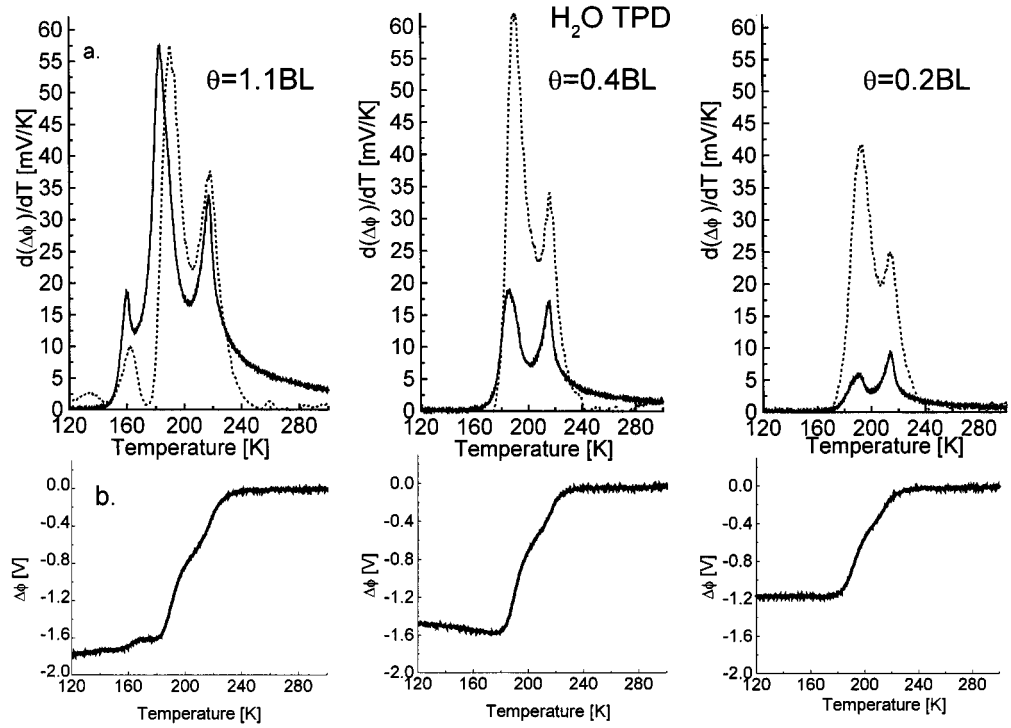

Figure 4. $\Delta p-$TPD (a) and $\Delta\varphi-$TPD (b) of H_2O from Ru(001) at initial coverages of 1.1 (left), 0.4 (middle), and 0.2 BL (right). Adsorption temperature was 82 K and the heating rate 2 K/s. The derivative of the $\Delta\varphi-$TPD ($d\Delta\varphi/dT$) is superimposed on the $\Delta p-$TPD (dashed line) reflecting the contribution of each of the adsorption sites to the measured $\Delta\varphi$. Note the shift of the A_2 peak in the $d\Delta\varphi/dT$ spectra at high coverages, as discussed in the text.

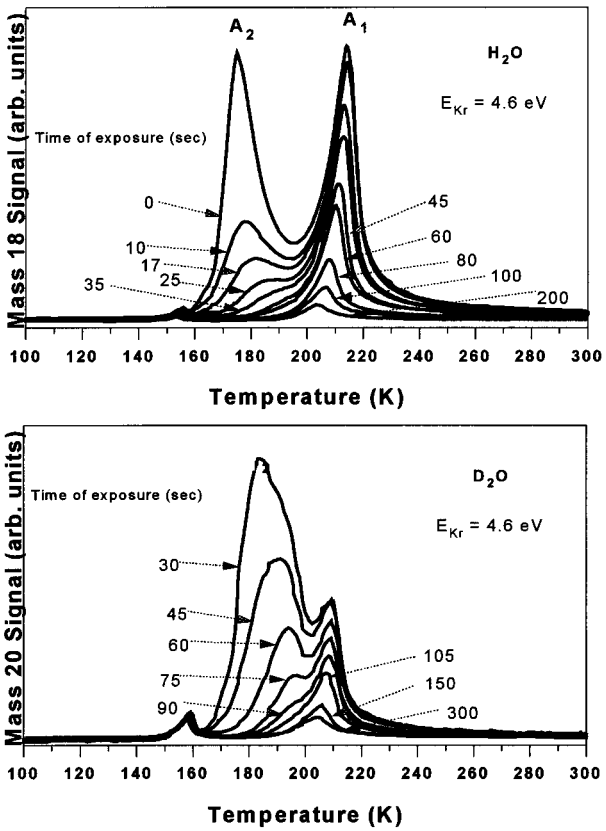

Figure 5. TPD of H_2O (upper figure) and D_2O (lower figure) following collision with Kr atoms at 4.6 eV for the indicated times of exposure. Initial coverage was 1 BL, adsorption temperature was 140 K, and heating rate was 2 K/s.

TPD spectra in Figure 5, were obtained after exposing the water-covered surface to the Kr beam for various periods of time, up to 300 s. We observed that water molecules in the A_1 state near 215 K are removed at much slower rate than were molecules in the A_2 state, regardless of the adsorption temperature (90 or 140 K). After exposing the surface for longer than 60 s in the case of H_2O and 100 s for D_2O at Kr beam of 4.6 eV, the only populated state that remained on the surface is the A_1 state and some icelike clusters desorbing near 150−160 K.

This, we believe, demonstrates that the A_1 sites are not populated from the A_2 state molecules during the TPD. The A_1 sites are apparently already populated independently upon adsorption at 90 K. The hypothesis that A_1 molecules are thermally populated from the A_2 state has been the basis for the attempt to explain the kinetic isotope effect in desorption of H_2O and D_2O from Ru(001).[13] On the basis of careful LEED study, the structure of the A_1 H_2O molecules was suggested to be composed of stable domain-stripes on the surface.[19] This unique structure could not be observed in the case of D_2O, for which a uniform overlayer structure was proposed.[16,17] To emphasize the similar response of both H_2O and D_2O to the CID process, as discussed above, TPD spectra following CID of both molecules after 60 and 90 s exposure to Kr beam at 4.6 eV are shown in Figure 6. The important point to note here is that for both H_2O and D_2O the A_1 state near 210 K, seems to be occupied without any population of the A_2 state, thought to be a necessary precursor state for its population.[13]

We conclude from the results shown in Figures 5 and 6 that A_1 sites are populated by both H_2O and D_2O upon adsorption. This is based on the fact that the A_1 molecules are exposed and can be seen by TPD, even if a complete removal of the A_2 molecules takes place following CID in both systems. This is a

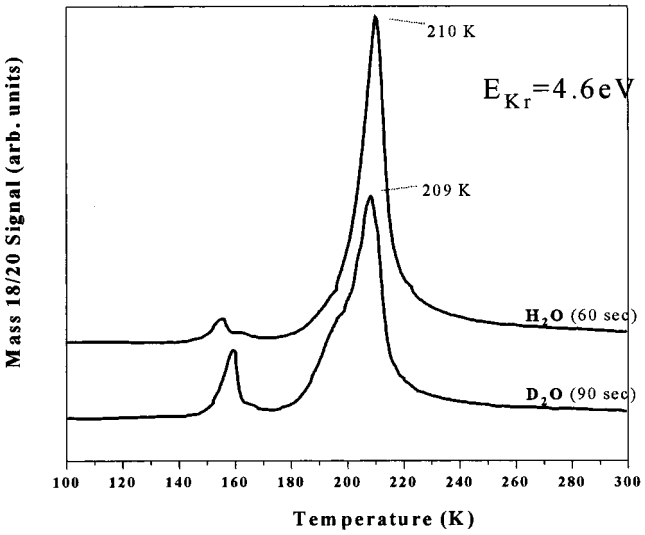

Figure 6. TPD of H_2O and D_2O following exposure to Kr atoms at 4.6 eV for the indicated time. Initial coverage, adsorption temperature, and heating rate were as in Figure 5.

rather different behavior than that in normal TPD, where both A_2 and A_1 sites are populated down to coverages less than 0.1 of a monolayer.

We may also conclude that our data do not support the unique structure suggested for A_1 H_2O molecules based on LEED investigation.[17] In this study, striped domains were proposed to explain the observed LEED. However, the CID process uniformly removes the A_2 molecules, and therefore it is not expected to maintain a striped structure for the A_1 molecules. Our CID results, therefore, are more simply explained on the basis of the classic icelike bilayer structure discussed earlier in the literature.[1,10]

In the case of D_2O, on the other hand, it seems that the A_1 peak is somewhat shifted to lower temperatures and therefore overlaps the A_2 state in the normal TPD. The origin for this shift cannot be explained on the basis of our experiments.

The cross section for CID as a function of the Kr incident kinetic energy for the two water molecule isotopes was measured. Threshold energies of 3.4 eV for H_2O and 3.8 eV for D_2O were found.[23] The higher threshold energy in the case of D_2O can be attributed to the stronger binding of this isotope to the surface, as shown by the higher desorption peak temperature of D_2O in the A_2 state (185 vs 175 K).

Consistent with the high threshold energy for the CID of water, we found an interesting observation regarding the icelike particles on the surface. It turns out that these ice clusters, found in the TPD spectra of H_2O and D_2O near 150−160 K, are practically insensitive to collisions with the energetic rare gases (see Figures 5 and 6). This is despite the fact these hydrogen-bonded particles are thermally less stable than the A_2 state molecules which are removed by the collisions. Collision energies up to 5.0 eV, an order of magnitude higher than the hydrogen-bond energy, do not seem to be sufficient to break these intermolecular bonds. This observation suggests that the hydrogen-bonded network is extremely efficient in dissipating high kinetic energies of rare gas colliders. The kinetic energy of the collider can be absorbed by the many inter- and intramolecular vibrational modes and other soft degrees of freedom within the ice 3D structure.

A recent CID study of hydrocarbons adsorbed on Au(111) has shown a good correlation between the threshold energy for the CID event and the extent of "softness" of the molecular

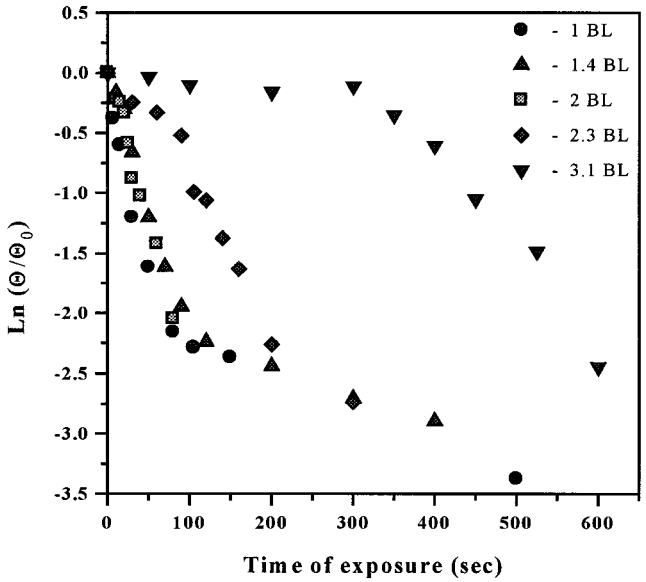

Figure 7. Removal rate of H_2O following CID with Kr atoms at 5.5 eV. The rate of removal is expressed in terms of relative coverage of remaining water molecules (Θ) relative to the initial indicated coverage (Θ_I) vs exposure time to the Kr beam.

network (internal degrees of freedom) that can dissipate the collision energy.[35] This is in sharp contrast to the case of "stiff" adsorbates such as nitrogen[31] and rare gases,[36] for which the threshold for CID is about twice the binding energy.

3.4. CID of Thicker Water Layers. The removal rate of water via CID as a function of layer thickness on Ru(001) reveals an interesting behavior. In Figure 7, this is shown as a result of Kr at 5.5 eV striking the water-covered surface. The removal rate is measured by the integrated TPD of the remaining adsorbed water molecules recorded following the exposure to the Kr beam. In Figure 7, the ratio Θ/Θ_I defines the water coverage remains after the exposure to the beam divided by the initial coverage, as determined by TPD. When plotted against the exposure time, it provides a relative measure of the removal rate. It is clearly seen that the removal rate becomes slower as the number of water layers increases. However, a most significant decrease in the removal rate is found at coverages above 2.5 BL. The initial slope in Figure 7, which represents the relative removal rate, decreases by an order of magnitude when comparing the removal rate of the first bilayer to that of the third bilayer. This observation is consistent with the discussion on the extremely inefficient CID of 3D ice clusters. It shows that unique stability is gained by the ice network as its thickness reaches 3 BL or higher. This observation suggests special packing and organization above this thickness. The model calculations by Witek and Buch,[21] who studied the structure and energetics of the first layers of water on a model metal surface, have indicated that a special rearrangement of the water layers takes place at the fourth bilayer. In addition, it was found that the fourth bilayer is more stable than the structure pertains to three bilayers or less. These calculations basically support our observation. The fact that in the calculations the extra stability is found at the fourth bilayer while in the experiment it seems that the third bilayer is already more stable is most probably within the expected uncertainty of the model calculation based on the unknown water−ruthenium potential-energy surface.

3.5. Nitrogen Molecules as Spectators Under the Ice. Nitrogen molecules were reported by us to be buried under layers of ice in an "igloolike" arrangement.[37] These caged nitrogen molecules eventually desorb in an explosive desorption manner near the onset for ice desorption at 165 K instead of their usual desorption peak at 105 K, in a very narrow desorption peak width of ca. 2 K.

We observed that between 1.5 and 4 BL the major shift in the desorption peak of nitrogen takes place, as demonstrated in Figure 2 of ref 37.

It looks as if the ice cage starts to close on the adsorbed nitrogen molecules near the second−fourth bilayers. It correlates nicely with the extra stability found at the third layer in the CID experiments reported above; see Figure 7. This observation is explained by the classical molecular dynamics simulations mentioned above.[21] In this study, a rearrangement of the water layers was observed near the fourth bilayer accompanied by extra stability. The restructure at the fourth layer consisted of a lateral shift of the top layer relative to the layers below, which is claimed to be the most stable packing at this coverage. The shift of the fourth layer may result in a partial blocking of the channel for desorption of nitrogen through the open hexagonal ice structure. It, therefore, explains the fact that near that coverage, desorption of nitrogen molecules is gradually blocked. As seen in Figure 2 of ref 37, as the ice layer gets thicker, the desorption peak of the caged nitrogen becomes narrower.

A correlation between the experimental and the theoretical model calculations is valid only if we assume that the adsorbed nitrogen does not interfere in a significant way with the hydrogen-bonded network of the adsorbed ice layers. Such an assumption was concluded to be reasonable based on work function change data taken during desorption of the caged nitrogen molecules.[37]

4. Summary

Initial adsorption and formation of water clusters upon adsorption on Ru(001) at 82 K has been monitored using work function change measurements. A kinetic model that accurately reproduces the experimental data suggests that at low coverages monomers with dipole moments of 2.2 D dominate among the adsorbed species. As coverage increases, the density of tetramers with a dipole moment of 0.92 D, gradually grow, becoming the most populated species at coverages above 0.4 BL. The effective dipole moment per water molecule in these clusters is 1.12 D for a dimer, 0.86 D for a trimer, and 0.92 D for a tetramer. These values imply that the adsorbed clusters prefer planar configuration parallel to the surface at coverages up to half of a bilayer.

Collision-induced desorption experiments of H_2O and D_2O adsorbed on Ru(001) were performed. A selective CID takes place, whereby only water molecules that adsorb at the A_2 state are removed with a threshold energy for removal near 3.4 eV for H_2O and 3.8 eV for D_2O. This value is more than 7 times higher than the binding energy of water to the metal or compared to the energy of the hydrogen bond. It demonstrate the extremely high efficiency of the hydrogen-bonded network of adsorbed water molecules in dissipating the collision energy.

CID of thicker ice layers indicates that a gradual stabilization takes place as the layer becomes thicker. At 3 BL, there is a sudden drop in the CID removal rate of the top water layer down to an order of magnitude slower than the removal rate of the first bilayer. This can be understood in terms of a significant stability of the ice hydrogen-bonded network at thicknesses above 3 BL. This observation is consistent with the onset of cage formation of adsorbed nitrogen under ice layers above 2−4 BL and with recent model calculations that explain both the onset for cage formation and the extra stability at the same layer thickness.

Acknowledgment. This work has been supported by the Israel Science Foundation and the German−Israel Foundation. The Farkas center is supported by the Bundesministerium fur Forschung und Technologie and the Minerva Gesellschaft fur die Forschung mbh.

References and Notes

(1) Thiel, P. A.; Madey, T. E. *Surf. Sci. Rep*. **1987**, *17*, 211.
(2) Madey, T. E.; Netzer, F. P. *Surf. Sci.* **1982**, *117*, 549.
(3) Pache, T.; Steinrük, H.-P.; Huber, W.; Menzel, D. *Surf. Sci*. **1989**, *224*, 195.
(4) Zinck, J. J.; Weinberg, W. H. *J. Vac. Sci. Technol.* **1980**, *17*, 188.
(5) Jupille, J.; Pareja, P.; Fusy, J. *Surf. Sci.* **1984**, *139*, 505.
(6) Madey, T. E.; Yates, J. T. Jr. *Chem. Phys. Lett*. **1977**, *51*, 77.
(7) Thiel, P. A.; Hoffmann, F. M.; Weinberg, W. H. *J. Chem. Phys*. **1981**, *75*, 5556.
(8) Thiel, P. A.; Hoffmann, F. M.; Weinberg, W. H. *Phys. Rev. Lett*. **1982**, *49*, 501.
(9) Kretzschmar, K.; Sass, J. K.; Bradshaw, A. M.; Holloway, S. *Surf. Sci*. **1982**, *115*, 183.
(10) Doering, D. L.; Madey, T. E. *Surf. Sci*. **1982**, *123*, 305.
(11) Williams, E. D.; Doering, D. L. *J. Vac. Sci. Technol*. **1983**, *A1*, 1188.
(12) Thiel, P. A.; DePaola, R. A.; Hoffmann, F. M. *J. Chem. Phys*. **1984**, *80*, 5326.
(13) Schmitz, P. J.; Polta, J. A.; Chang, S.-L.; Thiel, P. A. *Surf. Sci*. **1987**, *186*, 219.
(14) Coulman, D.; Puschmann, A.; Hoofer, U.; Steinrück, H.-P.; Wurth, W.; Feulner. P.; Menzel, D. *J. Chem. Phys*. **1990**, *93*, 58.
(15) Pirug, G.; Ritke, C.; Bonzel, H. P. *Surf. Sci*. **1991**, *241*, 289.
(16) Held, G.; Menzel, D. *Surf. Sci*. **1994**, *316*, 92.
(17) Callen, B. W.; Grifiths, K.; Kasza, R. V.; Jensen, M. B.; Theil, P. A.; Norton P. R. *J. Chem. Phys*. **1992**, *97*, 3760.
(18) Pangher, N.; Schmalz, A.; Haase J. *Chem. Phys. Lett*. **1994**, *221*, 189.
(19) Held, G.; Menzel, D. *Surf. Sci*. **1995**, *327*, 301.
(20) Held, G.; Menzel, D. *Phys. Rev. Lett*. **1995**, *74*, 4221.
(21) Witek, H.; Buch, V. *J. Chem. Phys*. **1999**, *110*, 3168.
(22) Nakamura, M.; Ito, M. *Chem. Phys. Lett*. **2000**, *325*, 293.
(23) Romm, L.; Livneh, T.; Asscher, M. *J. Chem. Soc*., *Faraday Trans*, **1995**, *91* (20), 3655.
(24) Bernal, J. D.; Fowler, R. H. *J. Chem. Phys.* **1933**, *1*, 515.
(25) Pauling, L. *J. Am. Chem. Soc.* **1935**, *57*, 2680.
(26) (a) Zeiri, Y.; Low, J. J.; Goddard, A., III. *J. Chem. Phys*. **1986**, *84*, 2408. (b) Zeiri, Y. *Surf. Sci*. **1990**, *231*, 408.
(27) Beckerle, J. D.; Johnson, A. D.; Ceyer, S. T. *Phys. Rev. Lett*. **1989**, *62* (6), 685.
(28) Szulczewski, G.; Levis, R. J. *J. Chem. Phys*. **1995**, *103* (23), 10238.
(29) Åkerlund, C.; Zoric, I.; Kasemo, B.; Cupolillo, A.; Buatier de Mongeot, F.; Rocca, M. *Chem. Phys. Lett.* **1997**, *270*, 157.
(30) Åkerlund, C.; Zoric, I.; Kasemo, B. *J. Chem. Phys.* **1998**, *109*, 737
(31) Romm, L.; Zeiri, Y.; Asscher, M. *J. Chem. Phys*. **1998**, *108* (20), 8605.
(32) Romm, L.; Zeiri, Y.; Asscher, M. *J. Chem. Phys*. **1999**, *110* (6), 3153.
(33) Pribble, R. N.; Zwier, T. S. *Science* **1994**, *265*, 75.
(34) Livneh, T.; Asscher, M. *Langmuir* **1998**, *14*, 1348.
(35) Libuda, J.; Scoles, G. *J. Chem. Phys.* **2000**, *112*, 1522.
(36) Kulginov, D.; Persson, M.; Rettner, C. T. *J. Chem. Phys.* **1997**, *106*, 3370.
(37) Livneh, T.; Romm, L.; Asscher, M. *Surf. Sci.* **1996**, *351*, 250.
(38) Lilach, Y.; Asscher, M., in preparation.